INFLUENCE OF GEOLOGICAL VARIATIONS ON LIGNITE DRYING KINETICS IN SUPERHEATED STEAM ATMOSPHERE FOR BELCHATOW DEPOSIT LOCATED IN THE CENTRAL POLAND

by

Anna SCIAZKO [a,b], ***Yosuke KOMATSU*** [b,c*], ***Marcin ZAKRZEWSKI*** [a], ***Taro AKIYAMA*** [c], ***Akira HASHIMOTO*** [c], ***Naoki SHIKAZONO*** [c], ***Shozo KANEKO*** [c], ***Shinji KIMIJIMA*** [b,c], ***Janusz S. SZMYD*** [a], ***and Yoshinori KOBAYASHI*** [c]

[a] Department of Fundamental Research in Energy Engineering, AGH University of Science and Technology, Krakow, Poland
[b] Division of Regional Environment Systems, Shibaura Institute of Technology, Saitama, Japan
[c] Institute of Industrial Science, The University of Tokyo, Tokyo, Japan

Original scientific paper
DOI: 10.2298/TSCI151111107S

Lignite-fired coal power plants suffer from a significant heat loss due to the high moisture content in this energy carrier. Water removal from fuel is an indispensable treatment for improving the combustion process, which will foster the efficient utilization of lignite. Superheated steam fluidized bed drying is expected for this purpose in a power generation sector. Understanding drying kinetics of lignite will greatly reinforce design process of a dryer. Physical features as well as the drying behaviour may be divergent among the lignite originated from different depths and positions in a certain mine. To reveal and clarify the influence of the geological features, the drying characteristics of several grades of lignite from the Belchatow mine in Poland were investigated. The attempts to clarify the influence of the divergent properties of the investigated samples on the drying kinetics in superheated steam were presented in this paper.

Key words: *lignite, low-rank coal, lignite drying, superheated steam drying, lignite upgrading*

Introduction

Lignite deposits are regarded as an important primary energy source and play strategic role in countries where the share of lignite in energy mix becomes a dominant level. Poland, one of those countries, lies their economy on the lignite power stations; more than 35% of gross electricity generation is accomplished by the lignite-fired power generation. However, the future of lignite utilization in power generation is currently difficult to determine because of the established energy policy in terms of regulating CO_2 emission, which was strictly relevant to the present EU program [1]. This hurdle is mostly connected to the inherent characteristics of this energy career. Lignite-fired power plants suffer from losing an extensive amount of heat in the combustion process due to the evaporation of a large amount of water kept in the structure of lignite physically and chemically. This heat loss deteriorates thermal efficiency of the plant and induces a large consumption of fuel. Reducing heat losses caused by high moisture content is likely a key in light of improving thermal efficiency of the lignite-fired power plants. Water removal thus has a significance in technological breakthrough for

* Corresponding author; e-mail: m610101@sic.shibaura-it.ac.jp

the advanced utilization of lignite in power generation sector, as it was shown in the study by Agraniotis *et al.* [2].

Among various types of proposed dewatering systems by means of mechanical, thermal or chemical methods, superheated steam fluidized bed drying (SSFBD) enables recovering latent heat from the water vaporization and is potentially capable of recovering part of sensible heat in a self-heat recuperative configuration [3]. This will greatly improve the power generation efficiency compared with traditional systems. It is also reported that this drying method can improve the grindability of dried lignite [4]. A superheated steam fluidized bed drying system has been designed on an industrial scale [5, 6]. Detailed specifications of a SSFBD, however, must be fixed in accordance with a certain grade of coal used in the located plant, as lignite-fired power plants are operated mostly with locally excavated lignite and different grades of lignite have various drying characteristics [7]. Previously, the drying kinetics of Australian and Polish lignite in superheated steam were investigated and dependencies of the drying kinetics on sample size and test temperature were discussed [8-10]. Importantly, the drying kinetics of lignite from a certain mine may imply the diversities of structure and composition along the depth of a seam. Those correlations must be further studied for the optimization of the SSFBD system. The present study focuses on investigating the influence of geological variation on the drying kinetics of lignite in atmospheric superheated steam conditions. Samples from several different depths of the Belchatow seam were used. The changes in weight (for calculating moisture content and drying rate), temperature profiles and surface observation of samples were simultaneously measured. The drying kinetics of several kinds of lignite samples extracted from the Belchatow lignite mine is discussed.

Belchatow lignite deposit

The Belchatow lignite deposit is located in the central Poland recognized as part of the Polish Lowlands, where majority of Polish lignite is found. The Belchatow mine is today the biggest lignite mine in Poland, responsible for 59% annual mining capacity. The Belchatow power plant, utilizing produced coal, has the capacity of the power 5.3 GW, among which 858 MW is supercritical unit assuring a high thermal efficiency. It supplies about 20% of the Polish power demand annually. The Belchatow power station is the largest thermal power station in Europe, the fourth largest fossil fuel and 28th largest power plant in the world.

Mining activity in the Belchatow area

The lignite deposits in the Belchatow area were found in 1960 and the coal is mined from 1980. Three mining fields are specified: the main fields of Belchatow and Szczercow and additional Kamiensk field. The lignite resource in the Belchatow mining field (the middle part of Kleszczow Graben) was estimated as over 1 billion tonnes and its exploitation is planned to be continued until 2019. The Szczercow mining field, located in the vicinity of the Belchatow field, is currently in the early mining phase – the production started in 2009. The Szczercow lignite deposit is estimated as 720 million tonnes and the output of the Szczercow field is currently substituting the descending mining capacity of the Belchatow field. The transfer of the mining infrastructure between fields assures continuous operation and the fuel supply for the Belchatow power plant until 2038. A satellite deposits of Zloczew are considered as a prospective resource. The Zloczew deposit is located in the 50 km distance from the current mine and is estimated as 450 million tonnes. The attractiveness of the deposit is determined by the relatively low investment cost. The existing Belchatow power plant can uti-

lize lignite on-site; moreover, the infrastructure and know-how of the present mine can be directly transferred to the new operation site. The Zloczew field has the capacity to provide fuel for the Belchatow power plant until 2055. In the future of the Belchatow lignite deposits, it will be important to increase the power generation efficiency with an advanced drying technology.

Geological origin of the Belchatow deposit

Generally, the Polish lignite deposits currently under exploitation, were created in the Miocene period [11]. The Belchatow deposit is originated in the lower Miocene and is categorized as the 3rd group of scinawa lignite seam (SLS-3). It has the form of one thick broad-spread sedimentation, of which the cross-section is presented in fig. 1. The shallow warm sea covering most of the Mesozoic area of the present Poland resulted in the Upper Jurassic (limestone content is the representative) and Cretaceous deposits (marls, geizes and diatomite are major petrographic sedimentary deposits). On the top of them, in the Kleszczow Graben where the Belchatow deposit is located, a tertiary lignite seam can be found along with Tertiary clays, such as kaolinite, illite and beidellite variety, and quartz sandstones. The calcium-rich Mesozoic basement rock induced the significant calcium contamination in the upper layers. Calcium can be found directly in lignite deposit in many forms, for example lacustrine chalk.

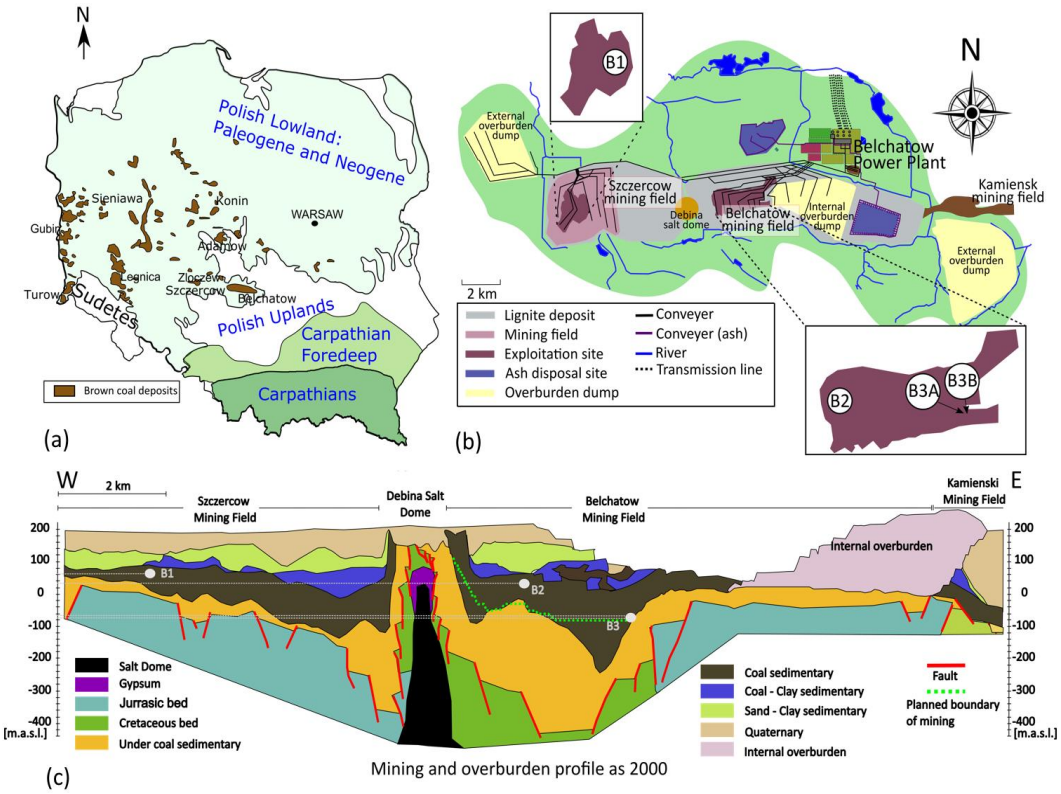

Figure 1. (a) Polish lignite deposits, (b) overview and (c) cross-section of the Belchatow lignite mine including three mining field of Szczercow, Bekchatow and Kamiensk

The investigated samples

In the previous study, the superheated steam drying behaviour of lignite from the Belchatow mine was presented [8]. The investigated sample was the representative sample from the annual excavation of the Belchatow mine in 2013. Along with the individual drying characteristics, the empirical model defining the total drying time and a thermodynamic deliberation concerning the drying rate in the initial stage of the process were proposed. This model is discussed later and implemented in the present study. It was noticed, that the superheated steam drying is highly dependent on the individual properties of the dried object [7]. Therefore, this study attempts to validate the proposed model for the lignite originated from the same deposit but characterized by various features. As it was explained, the mining is shifting from the Belchatow to the Szczercow mining field. For this reason, samples from both mining fields are studied to prove the applicability of the model for the current and future industrial purposes. The lignite sample presented in the previous work [8], representing the annual excavation in 2013 is included as Sample B2013. Sample B1 was extracted from the Szczercow field, while Samples B2, B3A and B3B were extracted from the Belchatow field. The depth of sampling varies from +60 m.a.s.l. to −78 m.a.s.l. and the precise location is given in the deposit cross-section (fig. 1). Despite the fact that the Belchatow deposit is considered as a uniform sedimentation, the individual properties of each sampling location vary among themselves and may influence the drying and industrial characteristics.

Physical and chemical properties of lignite samples

Proximate and ultimate analyses were carried out for all the extracted samples and presented in tab. 1. The total moisture is similar for all the investigated sample. A significant difference can be found on the amount of moisture in the air-dried basis; Sample B2013 contains the smallest amount of moisture, meanwhile the rest of the samples contains similar water percentage. The fuel ratio, presenting a ratio of fixed carbon to volatile matter, is 0.695, 0.622, 0.597 and 0.737 for Samples B2013, B1, B2 and B3B, respectively. The ash content lies in the range of 10.2-13.1 for Samples B2013, B1 and B2, while the ash content in Sample B3B is significantly small as resulted in 5.9. Along the depth of the seam, the ash content noticeably varies. Figure 2b shows the higher heating value (HHV). In form of the air-dried sample, the reference case, Sample B2013 shows the highest HHV, however, Sample B2013 contains less amount of moisture compared to the other samples. All of the samples have similar values in form of free moisture. Nevertheless, it is possible to categorize into two groups: one with Sample B2013 and B2 and the other with Samples B1 and B3B. Note that Samples B1 and B3B result relatively the higher HHV. This may be due to the lower ash content observed in those two particular samples. Figure 2a shows the chemical composition of ash in the investigated samples. A remarkable difference can be found on the content of SiO_2 and CaO. SiO_2, Al_2O_3 and CaO are substances found in the coal ash representing the sediment contamination. The high content of CaO in ash samples of all the investigated lignite can be attributed to the geological origin of lignite and the sedimentation conditions resulting in the chalk deposition associated with coal seam. The high alumina and silica content in the ash is similarly justified by kaolinites $Al_2Si_2O_5(OH)_4$ and quartz SiO_2 presence in the adjoining layers to the coal seam, which were also transferred directly to the lignite deposits and mixed with coal during the carbonization process and the sedimentation of organic matters. This may be the concern for the ash content in the samples from different geological locations. As seen in fig. 1c, Samples B1 and B2 are located on the upper part of the seam,

where the Quaternary sediment covers. On the other hand, Sample B3B is extracted rather close to the bottom of the lignite seam, below which the under coal sedimentary formed in the lower Miocene is located.

Similar characteristics in samples are found. However, noticeable differences appear with the increase of sampling depth and geographical location which may be substantially influenced by the stratigraphic, sedimentologic and petrologic features of the lignite seam formation.

Table 1. Proximate and ultimate analysis of Belchatow lignite samples

Contents [wt.%]	B2013	B1	B2	B3B	Contents [wt.%]	B2013	B1	B2	B3B
Total moisture	51.6	52.5	52.6	52.8	Ultimate analysis (dry basis: free moisture)				
Proximate analysis (air-dried basis)					C	56.9	57.3	54.5	62
Moisture	14.6	22.1	22.4	25.6	H	4.5	4.8	4.8	4.7
Fixed carbon	29.6	26	24.1	29.1	O	23.3	24.1	23.2	24.6
Volatile matter	42.6	41.8	40.4	39.5	N	0.7	0.51	0.5	0.7
Ash content	13.2	10.2	13.1	5.9	Ash	15.4	13	16.9	7.9

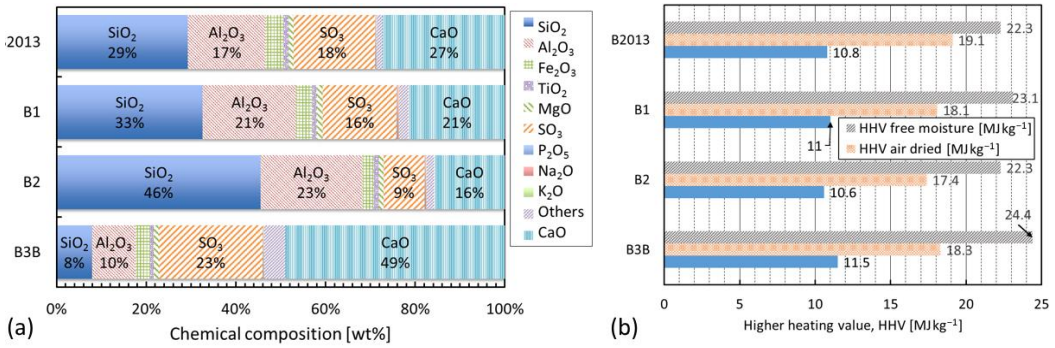

Figure 2. (a) Ash composition and (b) the higher heating value (HHV) in various forms of sample

Experimental investigations on superheated steam drying

Experimental set-up

The lignite drying in superheated steam was conducted with spherical lignite samples of 5 mm and 10 mm in diameter. An initial granulated sphere was roughly shaped with a knife. The shape of the sample was polished on a plate by rolling in a hole precisely punched with an electrical discharged machining. Polishing was carried out step by step in several sizes of holes to regulate the sample to the desired size. Interior temperature of a sample was measured with K-type thermocouples made of chromel and alumel. After the thermocouples were attached to the sample, they were rolled on a thin fragile glass rod (see fig. 3b).

Figure 3a shows the experimental set-up for the lignite drying test. After the preparation, the sample was set in the test section, where lignite was dried in a superheated steam atmosphere (see fig. 3a). The cylindrical test section, of which the diameter is 133 mm and the height is 152 mm, was adopted, operating with heaters to maintain the test temperature in the chamber. Pure water was degassed, pumped up by a liquid-delivery pump and provided to an evaporator and then a superheater. Steam was fed at an average velocity of 0.02 m/s to the test section.

The weight of the sample and its surface and interior temperatures were measured for the discussion of the drying characteristics. The weight was measured by an electronic balance that was connected with a metal suspension wire, on which the glass rod with the sample was hanged. The surface temperature was measured by a thermographic camera equipped with infrared bolometers in the range of wavelength detection from 8 to 12 μm. Thermograph data was calibrated on the basis of the assumptions of constant sample emissivity and constant test temperature as well as the sample characteristic temperature points achieved in the drying process (initial water evaporation at 100 °C and the final temperature). The surface observation was carried out with a video camera through an optical path to the drying chamber.

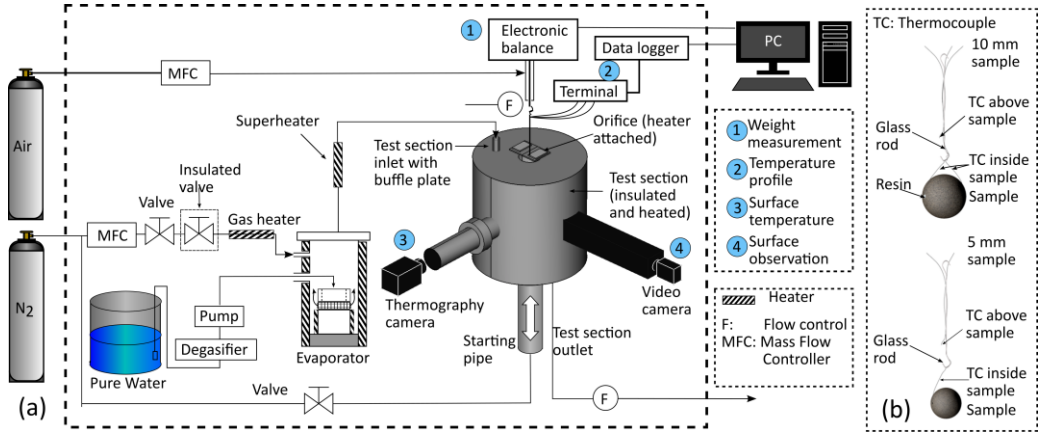

Figure 3. (a) Experimental set-up and (b) samples with 5 mm and 10 mm diameter

Experimental procedure

The samples were dried in the chamber where the temperature was kept at 110, 130, 150 and 170 °C. As drying temperature is maintained under 180 °C, it is assumed that volatilization and the decomposition of functional groups do not occur [12]. Thus, it can be treated that the change in the weight is caused by moisture removal. To define the exact moment of the start of the drying, a sample set on the glass rod was isolated from the superheated steam by raising the starting pipe. During this procedure, the starting pipe was filled with nitrogen. After lowering the starting pipe and exposing the sample to the superheated steam, changes in the weight and temperature profile of the lignite particle were consequently and simultaneously recorded in 1 s intervals. In order to verify the amount of residual water, the drying medium was switched to nitrogen, and the sample was dried for a certain time (depending on the test temperature and the size of the sample) enough to evaporate any additional moisture. The weight of the sample after nitrogen drying was regarded as the weight of the coal contained in the lignite (dry basis). Drying tests were conducted at least 3 times at each test temperature. Here, another important definition of the specific use of terms is noted; in this study, dry basis moisture content X [–] is defined as the ratio of the water weight W_w [kg] to the weight of the dried coal W_c [kg]:

$$X = \frac{W_w}{W_c} \tag{1}$$

whereas the ratio of the weight of the water to the initial weight of the sample is defined as the water percentage *WP* in wt.%:

$$WP = \frac{W_{\mathrm{w}}}{W_{\mathrm{ini}}} \times 100 = \frac{W_{\mathrm{w}}}{W_{\mathrm{w,ini}} + W_{\mathrm{c}}} \times 100 \tag{2}$$

where W_{ini} [kg] denotes the initial weight of the sample and $W_{\mathrm{w,ini}}$ [kg] stands for the initial weight of the water in the sample. The details can be found in the previous work [8].

Results and discussion

Superheated steam drying characteristics

The typical drying rate curve of a hygroscopic porous material can be decomposed for the typical periods dominated by the various phenomena:
(1) preheating period,
(2) constant drying rate period (CDRP),
(3) decreasing drying rate period (DDRP) phase 1,
(4) DDRP phase 2, and
(5) final drying.

Figure 4 presents the decomposition of drying behaviour for the exemplary case of a test with the 5 mm particle made of Sample B3B dried in superheated steam at 170 °C.

Preheating period

The weight of a sample increases due to the condensation of the superheated steam on its cold surface. As a result, the moisture content increases and the drying rate is below zero. The rapid increase of the surface and center temperatures, T_{S} and T_{C}, is observed (see fig. 4a). The condensation period is short and is continued until the surface reaches the saturation temperature T_{S} = 100 °C. At this moment, the weight and moisture in the sample is maximal in the overall drying process.

Constant drying rate period (CDRP)

The CDRP is characterized by the drying rate remaining at the constant level. Two phases can be pointed. In the first period of the CDRP(2a), the layer of water on the surface resulted from the condensation of the drying medium is evaporated. The surface temperature is kept constant, T_{S} = 100 °C; the center temperature reaches 100 °C and then is kept constant at this level ($T_{\mathrm{C}} \leq 100$ °C). The time-limiting step in this particular period is the evaporation of moisture from the sample surface defined by the drying conditions, such as the steam temperature and the particle size; the rate of the evaporation determines the rate of drying process. The CDRP(2a) finishes when the surface moisture is evaporated. In the CDRP(2b) the small rapid increase of T_{S} is observed, and after this the surface is kept at the constant temperature. The difference between T_{S} and T_{C} increases and shrinkage of the sample starts (see temperature curves in fig. 4a). The part of heat received by the sample increases the temperature in this region and the heat transfer to the interior of the sample proceeds. However, the evaporation occurs in the vicinity of the sample surface and the liquid water moves by capillary forces to the surface in the same proportion of the moisture evaporation (see fig. 4c). Drying rate is kept constant and is determined by the amount of heat exchanged with the superheated steam (see fig. 4d). The CDRP(2b) ends when drying rate starts decreasing and the

rapid increase in the T_S is observed. Note that the water removed in this period is categorized as free water.

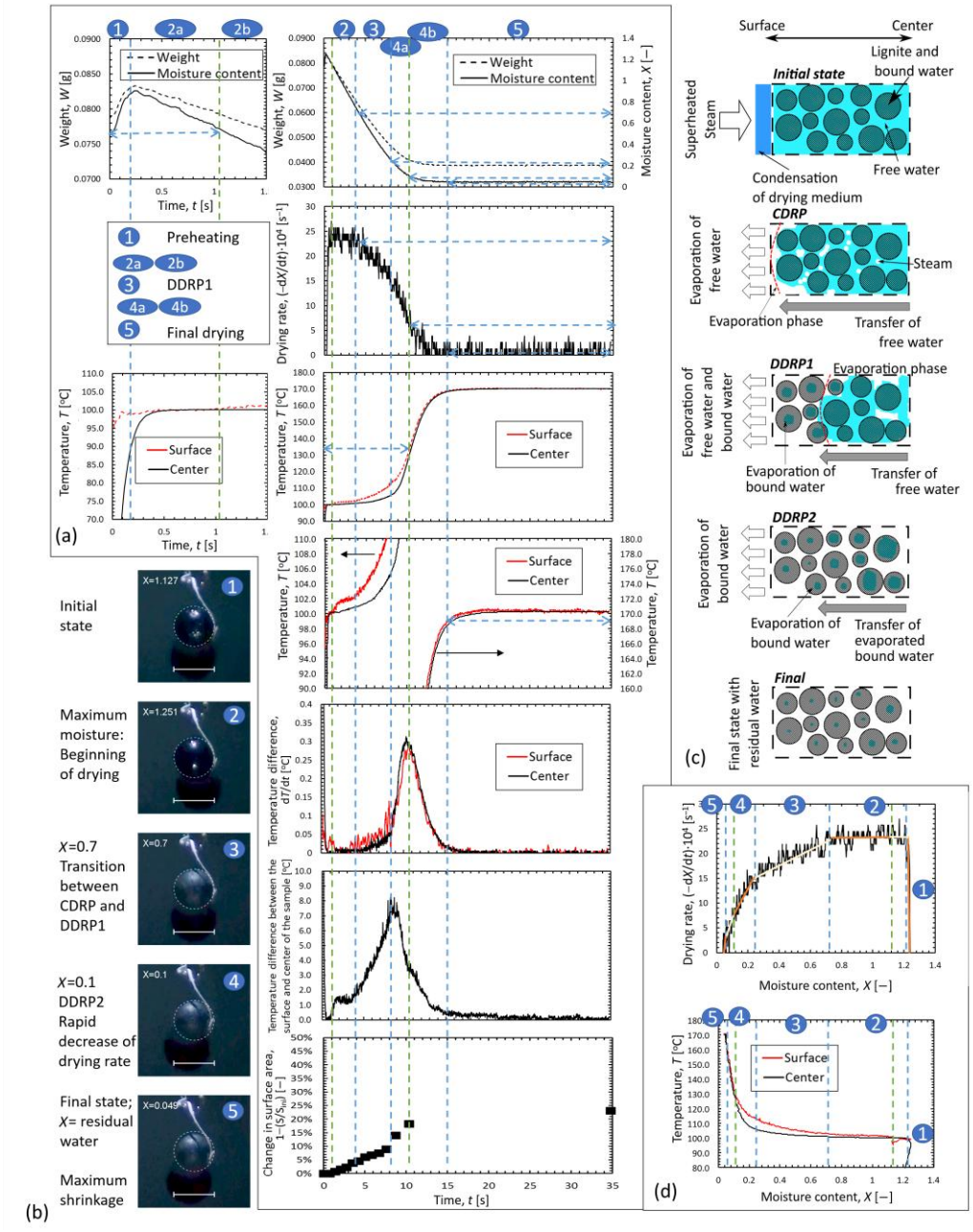

Figure 4. Drying characteristic of a 5 mm B3B lignite particle at 170 °C; (a) changes of sample weight, moisture content, drying rate, temperature and size with time, (b) surface observation and cracking, (c) schema of the various stages of the drying process and (d) drying rate and temperature change with time

Decreasing drying rate period 1 (DDRP1)

The weight and moisture content decrease slower than the previous period (see fig. 4d). The drying mechanism changes in this stage. The evaporation phase on the sample starts shifting towards the interior from the surface (see fig. 4c). As a result, mass transfer inside the sample involves the movement of water in the multiple-phase of liquid and gas. In this period, the hygroscopic water is evaporated. Hygroscopic water, the so-called bound water here, is strongly bonded with the lignite particle and its evaporation consumes more energy than that of the free water. The enthalpy change for the desorption of bound water (water evaporated above the saturation temperature) is reported to be the function of the moisture content [9]. This period is characterized by the extensive dewatering resulting in the cracking on the sample and shrinkage phenomena (see fig. 4b). The DDRP1 finishes when the increasing rate of the center temperature exceeds that of the surface temperature. As the result, the temperature difference between the surface and center reaches its maximum and starts to decrease (see fig. 4a).

Decreasing drying rate period 2 (DDRP2)

The decrease of the drying rate in DDRP2 is more rapid than during the DDRP1. The energy-consuming process of the evaporation of bound water is continued. The progressing shrinkage closes the cracks as it can be observed in fig. 4b. The DDRP2(4a) finishes, when the speed of temperature change achieves maximal value. During second part, DDRP2(4b) the temperature increase is decelerated, so do the dewatering speed. The DDRP2(4b) finishes once the temperatures inside the sample stabilizes at the test temperature (see fig. 4a).

Final drying period

The water strongly bonded with lignite is evaporated and the evaporation is continued until the residual water is reached $X = X_R$ defined by the surroundings. The temperatures of the sample reach the temperature of the superheated steam. The drying rate decreases close to zero, due to the difficulties of evaporation of the chemically bonded water. The final drying rate period is the longest among others and it gives the smallest improvement in the quality of lignite. Generally, the consecutive drying periods are longer, demand a large amount of heat supply, and give only a small improvement in the quality of the processed fuel. The most dominating and technologically important periods are the CDRP and DDRP1.

Figure 5 shows the exemplary of a drying test carried out with Sample B1 in superheated steam, of which temperature was 150 °C; 5 mm and 10 mm lignite particles are used in fig. 5a and 5b, respectively. The test was repeated at least 3 times with the samples made of randomly chosen block of lignite. Even in a single test condition, the influence of variation between the used lignite samples can be seen on the initial moisture content and the following drying behaviour. The enlargement in the particle size noticeably decreases the drying rate and elongate the drying time.

The initial moisture is a very important factor to distinguish the drying behaviour. The test with the highest initial moisture content results in the highest drying rate and the longer CDRP, and this increases the temperature gradient between the surface and center of the sample. Figure 6 shows the comparison of the drying behaviour observed with the 5 mm lignite particles made of Samples B2013, B1, B2, B3A and B3B. The presented tests were randomly chosen. The drying behaviour is very similar to each other though the initial mois-

ture content is in the range of 0.83-1.42. Sample B1 seems to be most water-rich sample among the investigated samples and shows a higher drying rate, whereas Sample B2013 contains the lowest moisture and results in the lowest drying rate. The influence of individual features of samples can be found on the represented cases. In the next subsection, the influence of individual features will be evaluated and explained quantitatively, using sensitivity analysis.

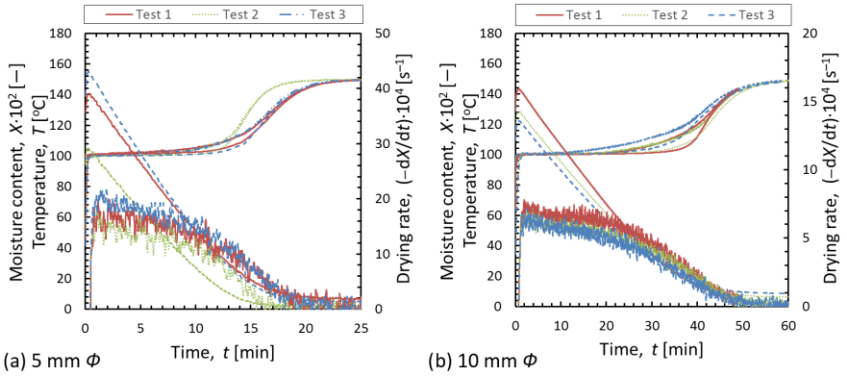

Figure 5. Drying kinetics at the test temperature of 150 °C for Sample B1 with the particle diameter of (a) 5 mm and (b) 10 mm

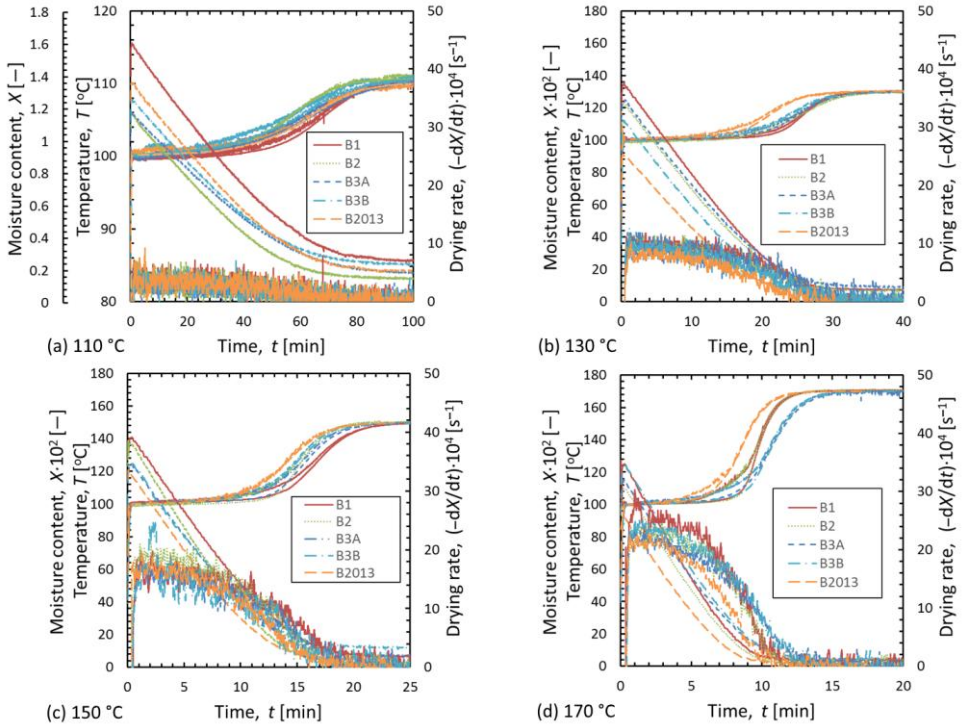

Figure 6. Drying behaviours of representative 5 mm lignite particles from Samples B2013, B1, B2, B3A and B3B in test temperatures of (a) 110 °C, (b) 130 °C, (c) 150 °C, and (d) 170 °C

Influence of individual features on drying characteristics

Despite the variation between the investigated samples, the general conclusion can be attempted. The correlation between the density and moisture content at the initial state, as-received basis, measured for all the investigated samples is presented in fig. 7. With the increasing depth of sampling, the initial water percentage is decreasing. This suggests a higher coalification level with the increase of the depth in the seam. The deviation of water measurement decreases with the depth, suggesting a more uniform local structure of the deposit. The variation of densities can be resulted from the ash contamination in lignite, and its local distribution influencing the densities of the investigated particles. Additionally, the density is deviated by the individual moisture content. Figure 8 presents the averaged value of the residual water remaining in all the investigated samples and drying time. The different values on the residual water are determined by the test conditions and decrease with increasing superheated steam temperature. The highest residual water is associated with Sample B3, while the lowest with Samples B2 and B2013. The tendency seems to be correlated with the ash concentration in lignite; a higher ash concentration results in a lower residual water. On the other hand, the drying time does not show the clear difference. The drying time is determined by both factors: the rapid dewatering in the CDRP and the DDRP1 and the slow removal of the bound water in the DDRP2.

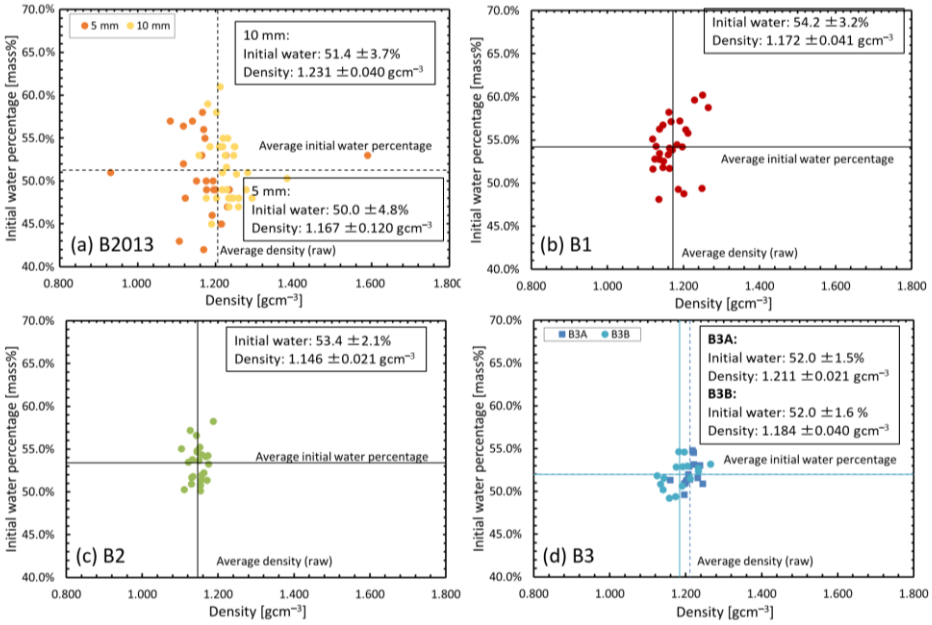

Figure 7. Density and initial water percentage for lignite; (a) B2013, (b) B1, (c) B2, (d) B3A, B3B

From a practical point of view, the most significant drying period is the initial drying, resulting in the revolutionary increase in the fuel quality. In the previous study [8], the thermodynamic analysis was proposed to determine the drying rate during the CDRP. The formula correlating the dry bulk density of lignite $\rho_b = m_1/V_{ini}$, the approximation of the heat transfer coefficient, derived from thermodynamic consideration in [8] $h = f(T_{test}, d)$, and the drying rate is:

$$\frac{\mathrm{d}X}{\mathrm{d}t_{\mathrm{CDRP}}} = \frac{6h(T_{\mathrm{test}} - T_{\mathrm{s}})}{\Delta H \rho_{\mathrm{b}}} \frac{1}{d} \tag{3}$$

where h, d, T_{test}, and T_{s} stand for heat transfer coefficient, the sample diameter, the test temperature and the surface temperature of the sample. $\Delta H = L = -2.256$ MJ/kg represents the enthalpy change necessary for the vaporization of the free water (at 100 °C and 101.3 kPa). The model is capable of predicting the drying rate during the CDRP only on the basis of the particle size and test temperature, with the assumption that the volatilization of dry matter does not occur. The simulated drying rates in the CDRP are compared to the experimental results in fig. 9, which shows good agreement. The influence of the size and the test temperature is addressed. The comprehensive sensitivity analysis for the size and temperature dependences is presented in fig. 10 for chosen dry bulk densities of lignite that equals 500 and 700 kg/m^3. The decrease in the size results in a large improvement in the drying rate. The increasing superheated steam temperature fosters a higher drying rate and the influence is especially visible in the case of a small dried particle. The dry bulk density is determined by the moisture and ash contents. A lower dry bulk density boosts the effect of the process parameters for the drying rate.

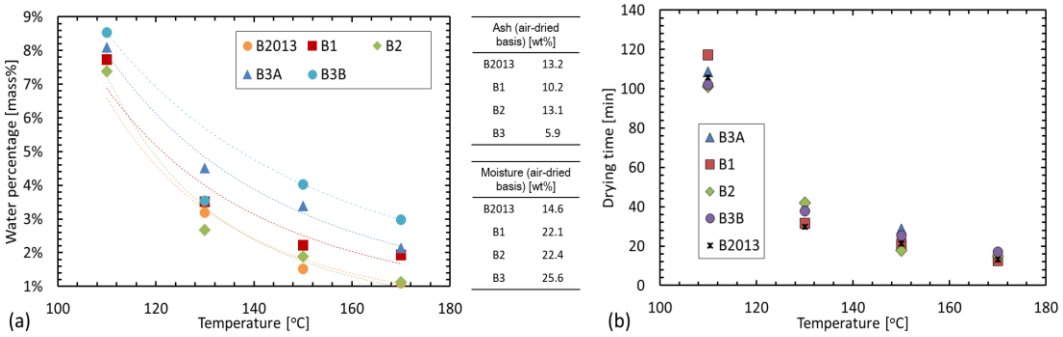

Figure 8. (a) averaged residual water and (b) averaged drying time of 5 mm diameter lignite samples in correlation with test temperature

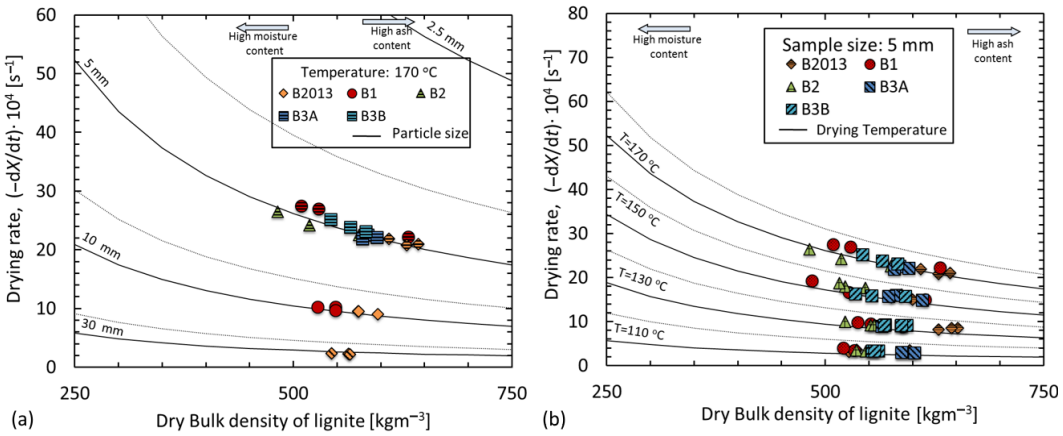

Figure 9. Influence of (a) diameter of the sample and (b) test temperature for the drying rate; experimental results indicated by points, prediction indicated by lines

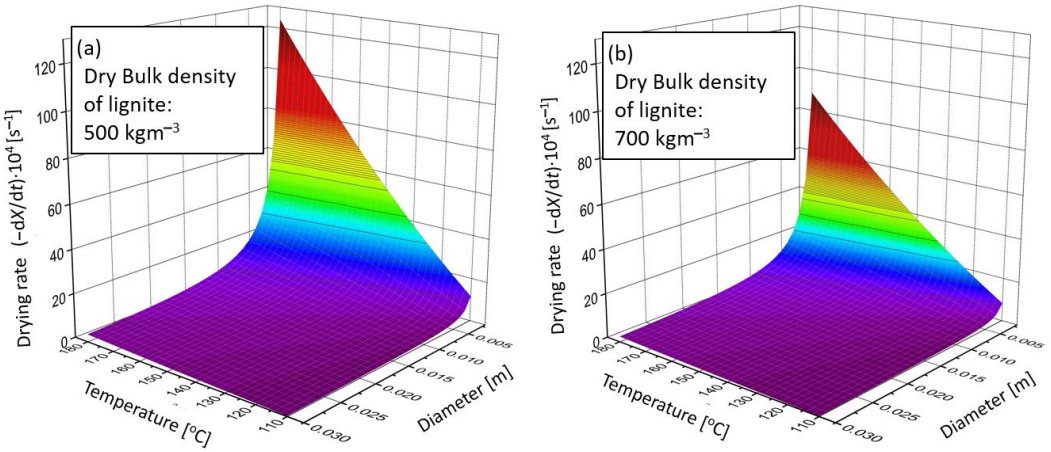

Figure 10. Influences of the drying parameters for the drying rate at CDRP with the sample of which the dry bulk density at (a) 500 kg/m^3 and (b) 700 kg/m^3

Conclusions

The present paper carried out the fundamental drying kinetic research of several grades of lignite, extracted from the Belchatow mine in Poland. Coal properties were investigated to clarify the representative characteristics of the investigated samples. The revealed various coal properties may influence the drying behaviours in the drying tests in superheated steam atmosphere. Throughout the carried out attempts, it can be concluded that the one thick broad-spread seam in the Belchatow mine may have relatively homogeneous structure. This fact allows for applying the proposed and generalized superheated steam drying model including the influence of steam temperature and particle size. The conducted research proves the validity of the proposed model for approximation of drying rate in the CDRP, and emphasises the impact of individual properties of lignite. Those parameters are crucial in designing and optimizing of the SSFBD system. The installation of the SSFBD to the existing plants and to the new investments can greatly improve the power generation efficiency.

Acknowledgment

This study was financially supported by the Japan Coal Energy Center (JCOAL) and the Polish National Centre for Research and Development (NCBR Project: I_POL-JAP, SSD-4-LRC).

References

[1] Batas-Bjelic, I., *et al.*, A Realistic EU Vision of a Lignite-based Energy System in Transition: Case Study of Serbia, *Thermal Science*, *19* (2015), 2, pp. 371-382
[2] Agraniotis, M., *et al.*, Investigation of Pre-drying Lignite in an Existing Greek Power Plant, *Thermal Science 16* (2012), 1, pp. 283-296
[3] Fushimi, C., *et al.*, Novel Drying Process Based on Self-Heat Recuperation Technology, *Dry. Technol.*, *29* (2010), 1, pp. 105-110
[4] Jangam, S. V., *et al.*, A Critical Assessment of Industrial Coal Drying Technologies: Role of Energy, Emissions, Risk and Sustainability, *Dry. Technol.*, *29* (2011), 4, pp. 395-407
[5] Klutz, H. J., *et al.*, WTA Fine Grain Drying: Module for Lignite-fired Power Plants of the Future – Development and Operating Results of the Fine Grain Drying Plant, *VGB Power Tech*, *86* (2006), 11, pp. 57-61

[6] Klutz, H., *et al.*, The RWE Power WTA Process (Fluidized Bed Drying) as a Key for Higher Efficiency, *Gornictwo I Geoinzynieria (AGH J. Min. Geoengin.)*, *35* (2011), 3, pp. 147-153
[7] Mujumdar, A. S., *Superheated Steam Drying*, Handb. Ind. Dry., CRC press, Boca Raton, Fla., USA, 2006, pp. 439-452
[8] Komatsu, Y., *et al.*, An Experimental Investigation on the Drying Kinetics of a Single Coarse Particle of Belchatow Lignite in an Atmospheric Superheated Steam Condition, *Fuel Process. Tech.*, *131* (2015), Mar., pp. 356-369
[9] Kiriyama, T., *et al.*, Experimental Observations and Numerical Modeling of a Single Coarse Lignite Particle Dried in Superheated Steam, *Mater. Trans.*, *54* (2013), 9, pp. 1725-1734
[10] Kiriyama, T., *et al.*, Size Dependence of the Drying Characteristics of Single Lignite Particles in Superheated Steam, *Metall. Mater. Trans. E.*, *1* (2014), 4, pp. 349-363
[11] Widera, M., Changes of the Lignite Seam Architecture − A Case Study from Polish Lignite Deposits, *Int. J. Coal Geol.*, *114* (2013), July, pp. 60-73
[12] Kopp, O. C., Harris, L. A., Initial Volatilization Temperatures and Average Volatilization Rates of Coal – Their Relationship to Coal Rank and other Characteristics, *Int. J. Coal Geol.*, *3* (1984), 4, pp. 333-348

Paper submitted: November 11, 2015
Paper revised: March 27, 2016
Paper accepted: April 6, 2016